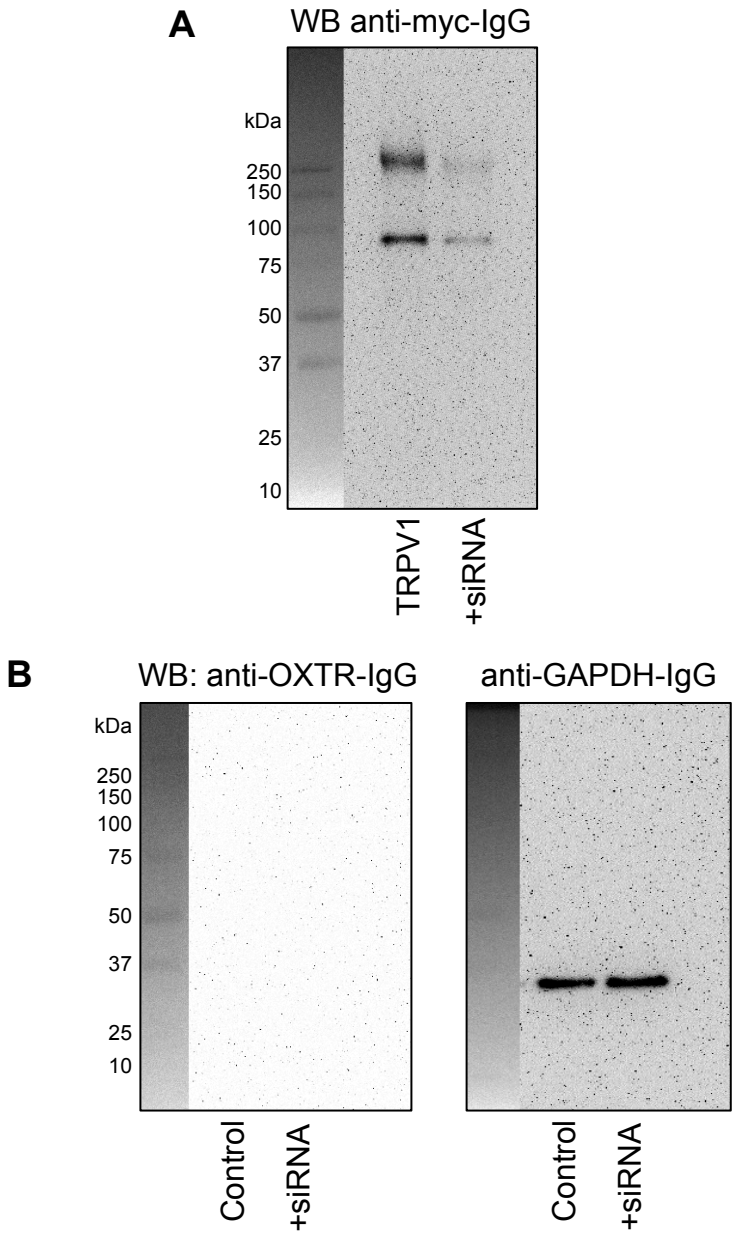

Figure S1: Protein expression levels after siRNA introduction. Related to Fig. 1.

A, Western blot (WB) displays TRPV1 protein expression levels in the control HEK-293 cells stably expressing TRPV1 and after introducing TRPV1-specific siRNA (Santa Cruz Biotechnology, Dallas, TX). The cells were transfected with 1 µg TRPV1-siRNA or control one using effectene reagent from Qiagen. After 44 h of growth, cells were washed once with PBS and detached from the plate by trypsin. Equal amounts of control and TRPV1-siRNA transfected cells ($1x10^5$ per sample) were used for WB detection of TRPV1. Cells were lyzed with 2X SDS-loading buffer, incubated at 95 °C bath for 15 minutes, and separated on 10% gel (BioRad). Blocking was done with 10 % milk for 1 h, following 2.5 h incubation with mouse anti-Myc antibody (4 µl per 8 ml of blocking buffer) and 1 h incubation with anti-mouse HRP-conjugated secondary antibodies, at room temperature. The chemiluminescence signals were obtained by using ECL Western Blotting Substrate (Thermo Scientific™ Pierce™).

B, WB was done to detect oxytocin receptor OXTR expression in the control F-11 cells and cells after introducing OXTR-specific siRNA (Santa Cruz Biotechnology, Dallas, TX). The cells were transfected with 1 µg OXTR-siRNA or control using effectene reagent from Qiagen. After 44 h of growth, cells were washed once with PBS and detached from the plate by trypsin. Equal amounts of control and OXTR-siRNA transfected cells ($1x10^5$ per sample) were used for WB detection of OXTR. We did not detect noticeable expression of OXTR levels in F-11 cells, which suggests that OXTR is present at low abundance levels (number of experiments n = 3). As a control we re-developed the WB with antibodies against GAPDH, which was detected at its predicted molecular mass of ~36 kDa.

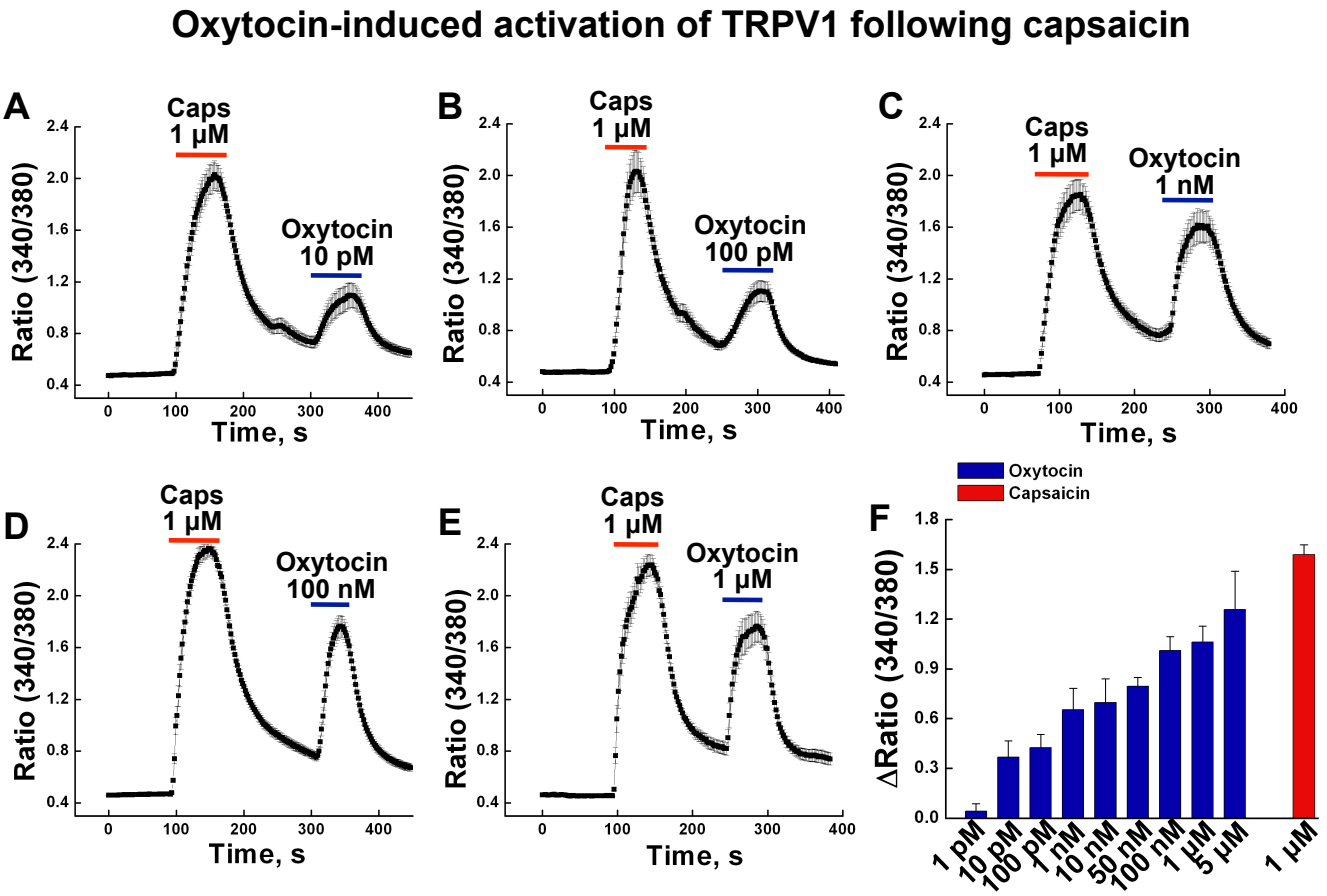

Figure S2: Oxytocin-induced potentiation of TRPV1 following capsaicin application. Related to Fig. 1.

Ca^{2+} imaging experiment performed on HEK-293 cells stably expressing TRPV1 channels: **A**, 10 pM oxytocin-induced activation of TRPV1 following 1 µM capsaicin application ($n_{exp.} = 3$, $n_{cells} = 71$). **B**, 100 pM oxytocin-induced TRPV1 response, following 1 µM capsaicin application ($n_{exp.} = 3$, $n_{cells} = 74$). **C**, 1 nM oxytocin-induced TRPV1 response, following 1 µM capsaicin application ($n_{exp.} = 3$, $n_{cells} = 64$). **D**, 100 nM oxytocin-induced TRPV1 response, following 1 µM capsaicin application ($n_{exp.} = 3$, $n_{cells} = 87$). **E**, 1 µM oxytocin-induced TRPV1 response, following 1 µM capsaicin application ($n_{exp.} = 3$, $n_{cells} = 80$). **F**, The summary presents the mean under all the conditions. All error bars stand for ±s.e.m.

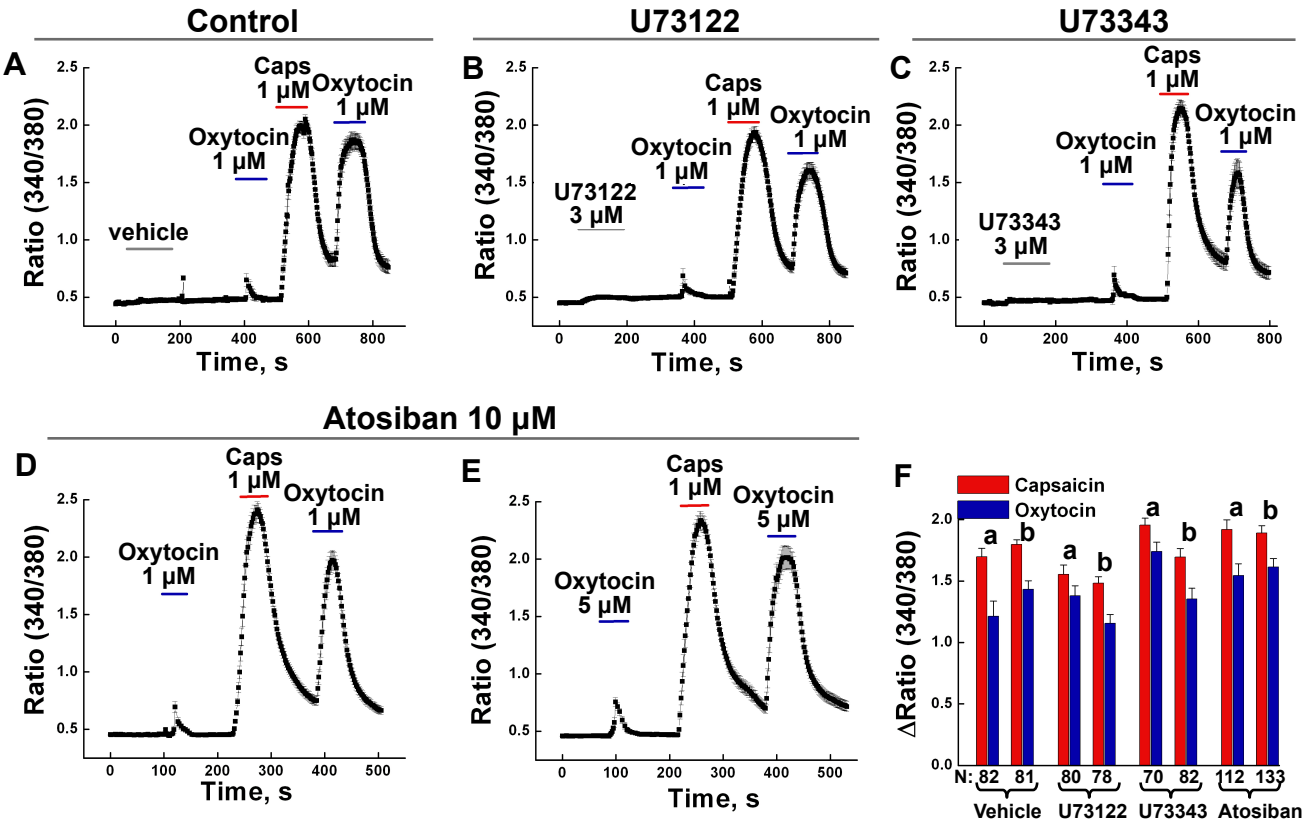

Figure S3: Oxytocin-evoked TRPV1 activity in the presence of PLC and OTRX inhibitors. Related to Fig. 1.

Ca^{2+} imaging experiment performed on HEK-293 cells stably expressing TRPV1 channels: **A**, cells were treated for 2 min with the vehicle, ethanol, at final concentration of 0.6%, washed for 2 min, followed by capsaicin (1 μM) and oxytocin (1 μM) applications ($n_{exp.} = 5$, $n_{cells} = 82$). **B**, cells were treated for 2 min with 3 μM of PLC inhibitor U73122, washed for 2 min, followed by capsaicin (1 μM) and oxytocin (1 μM) applications ($n_{exp.} = 6$, $n_{cells} = 80$). **C**, cells were treated for 2 min with 3 μM U73343 (as a control to U73122 treatment), washed for 2 min, followed by capsaicin (1 μM) and oxytocin (1 μM) applications ($n_{exp.} = 5$, $n_{cells} = 70$). **D**, cells were pretreated for 30 min with 10 μM of Oxytocin Receptor inhibitor atosiban, followed by capsaicin (1 μM) and oxytocin (1 μM) applications ($n_{exp.} = 7$, $n_{cells} = 112$). **E**, cells were pretreated for 30 min with 10 μM atosiban, followed by capsaicin (1 μM) and oxytocin (5 μM) applications ($n_{exp.} = 7$, $n_{cells} = 133$). **F**, The summary presents the mean under all the conditions: "**a**" columns present 1 μM oxytocin applications following 1 μM of capsaicin; "**b**" columns present 5 μM oxytocin applications following 1 μM of capsaicin. All error bars stand for ±s.e.m.

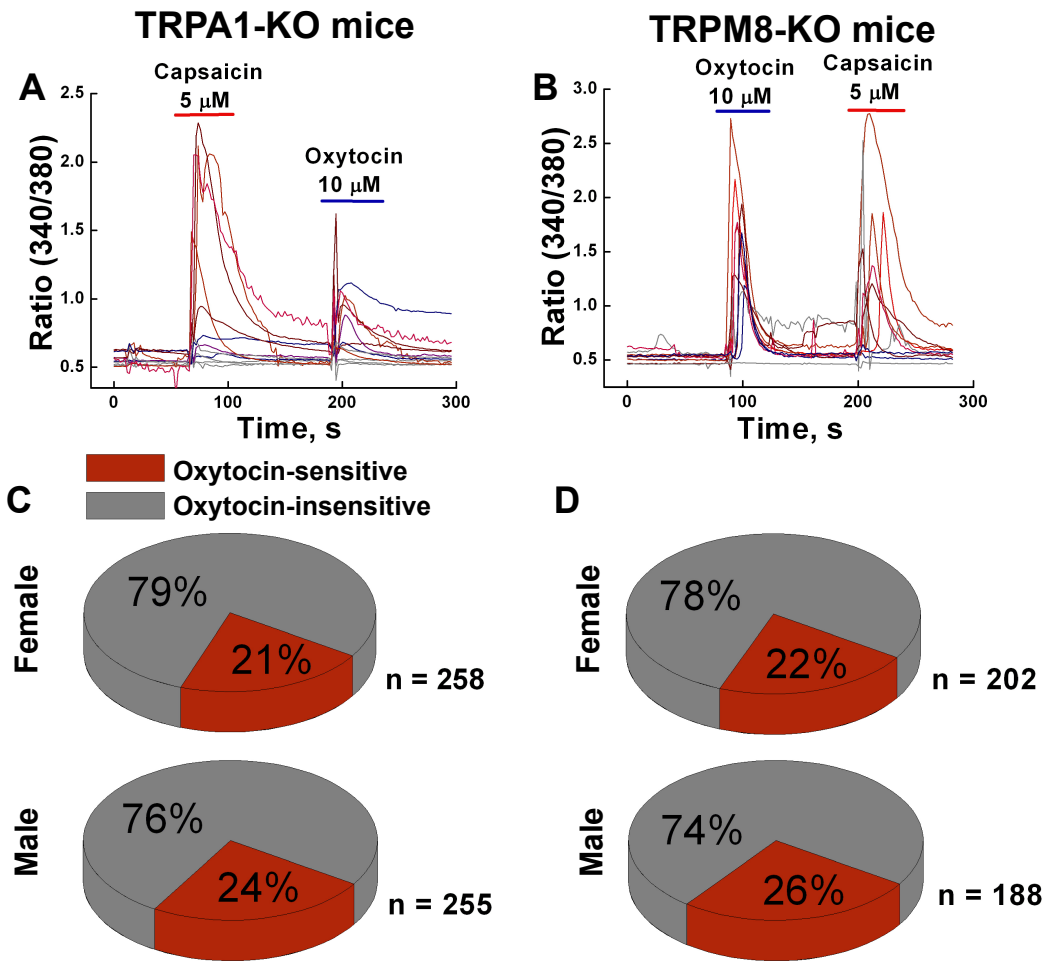

Figure S4: Oxytocin sensitivity in DRG neurons isolated from TRPA1$^{-/-}$ and TRPM8$^{-/-}$ mice. Related to Fig. 2.

A, Representative traces of the oxytocin- and capsaicin-elicited Ca^{2+} responses obtained from the DRG neurons of TRPA1$^{-/-}$ male mouse (a total number of measurements for both males and females $n_{exp.} = 18$). **B**, Representative traces of oxytocin- and capsaicin-elicited Ca^{2+} responses obtained from the DRG neurons of TRPM8$^{-/-}$ female mouse (a total number of measurements for both males and females $n_{exp.} = 24$). **C** and **D** panels show pie graphs of the distribution of the oxytocin-sensitive and oxytocin-insensitive DRG neurons isolated from the TRPA1$^{-/-}$-female ($n_{cells} = 258$), TRPA1$^{-/-}$-male ($n_{cells} = 255$), TRPM8$^{-/-}$-female ($n_{cells} = 202$), and TRPM8$^{-/-}$-male mice ($n_{cells} = 188$).

TRPV1 protein purification and mass spectrometry

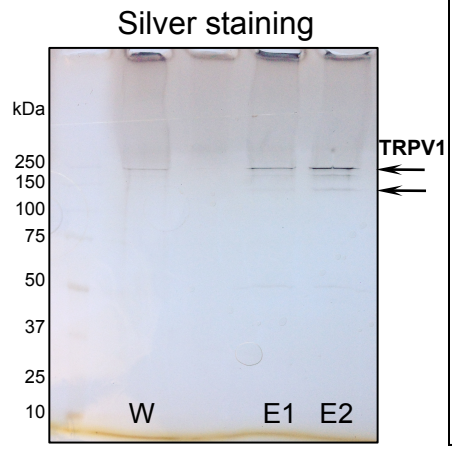

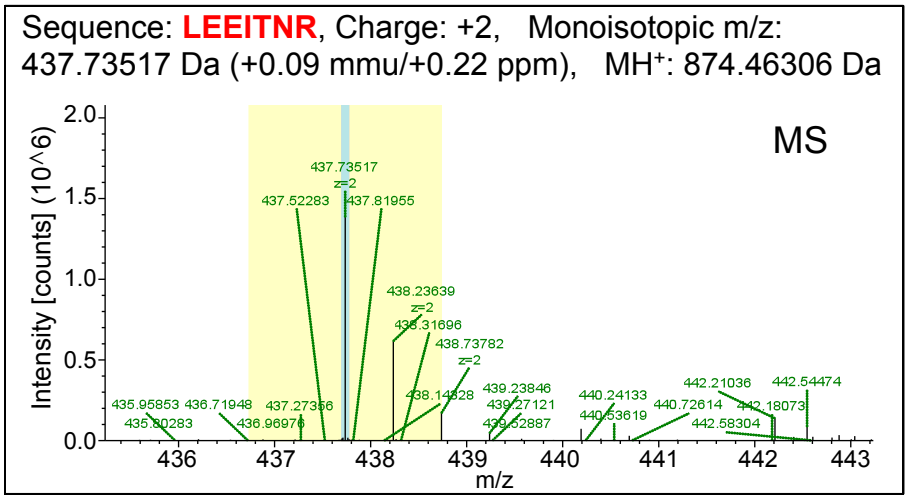

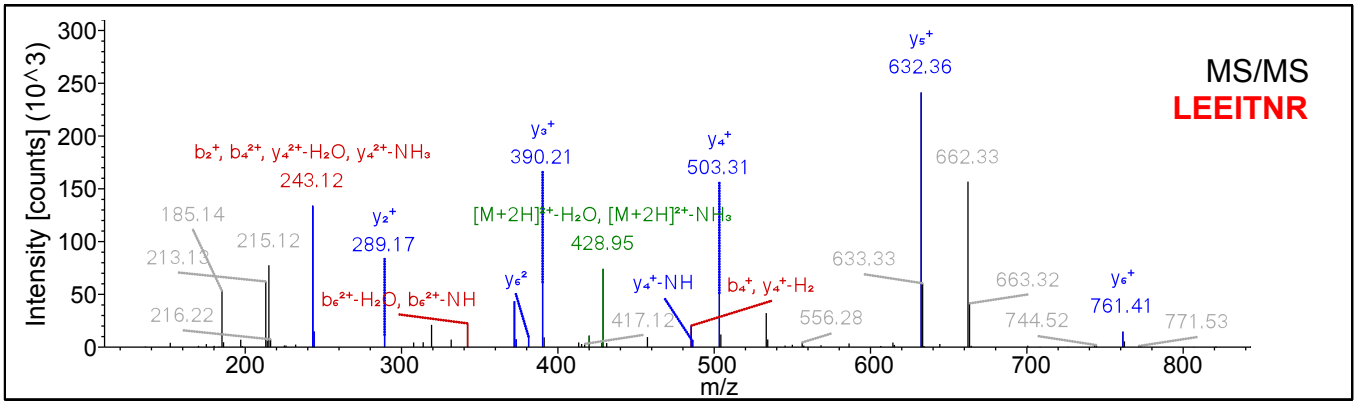

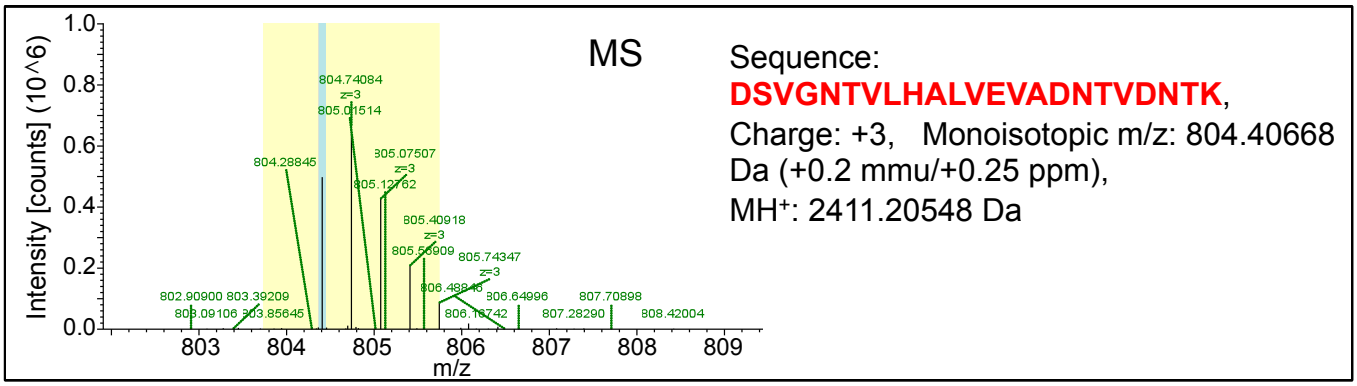

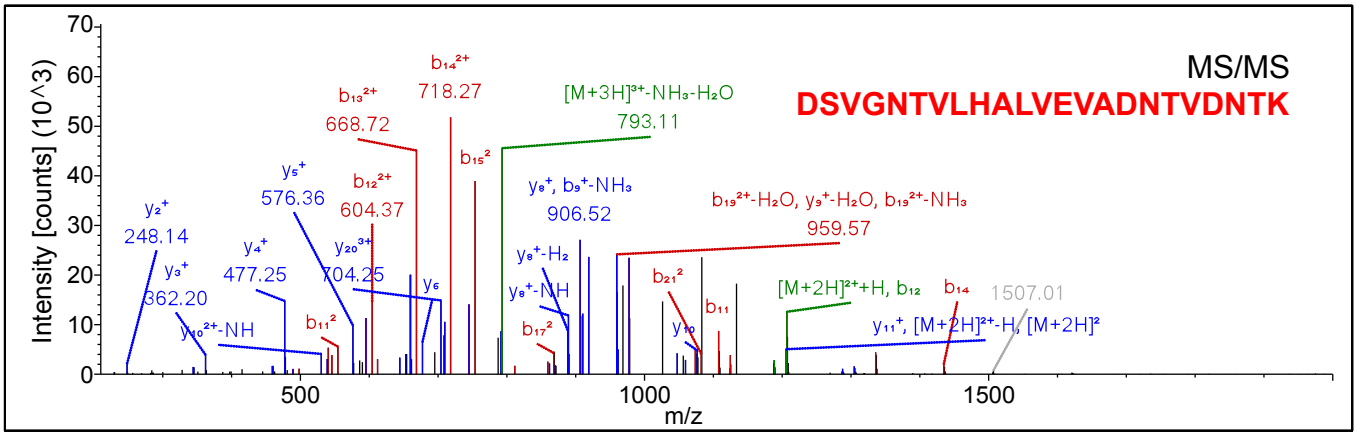

Figure S5: TRPV1 protein purification and mass spectrometry. Related to Fig. 4.

The Myc-tagged TRPV1 protein was purified by immunoprecipitation using monoclonal Myc-antibody (Sigma-Aldrich). Silver stained 10 % gel displays TRPV1 bands corresponding to the TRPV1 dimers and monomers, indicated by arrows. The letters indicate samples of wash (W), eluates (E), and left column presents markers. TRPV1 purified in the presence of 0.03% lauryl maltose neopentyl glycol (LMNG) preferably migrates on the gel in the form of dimers, and less in the form of monomers, for more details see (Lukacs et al., 2013).

The TRPV1 protein identity, prevalence, and purity in the obtained samples were validated using liquid chromatography mass spectrometric (LC-MS/MS) analysis. All bands present on the gel were excised and screened, where TRPV1 was present at the high abundance level. Representative MS and MS/MS spectra of the TRPV1 peptides are demonstrated in the figure.

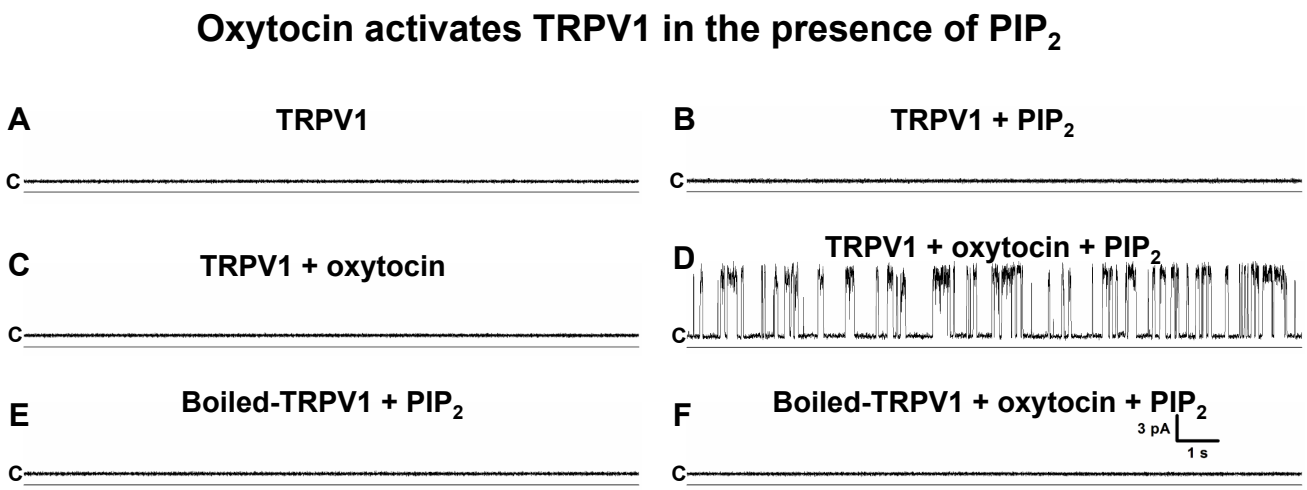

Figure S6: Oxytocin activates TRPV1 in the presence of PIP_2. Related to Fig. 4.

Representative TRPV1 channel traces obtained at different conditions in planar lipid bilayers. **A**, Representative traces of TRPV1 incorporated into planar lipid bilayers alone, and **B**, in the presence of PIP_2 (n = 25, with 2-5 h waiting time). **C**, TRPV1 incorporated in the bialyers in the presence of 0.5 μM oxytocin alone (n = 10, with at least 3 h waiting time), and **D,** after the addition of 5 μM PIP_2 (total number of events analyzed is 27,573; n = 13). Panels **E** and **F** demonstrate lack of TRPV1 channel activity in the presence of oxytocin and PIP_2 when the TRPV1 protein before incorporation to the bilayers was boiled for 30 min in the water bath (n = 5). All representative traces were obtained at 100 mV. The closed state indicated as letter "c" and is shown on the left of the traces.

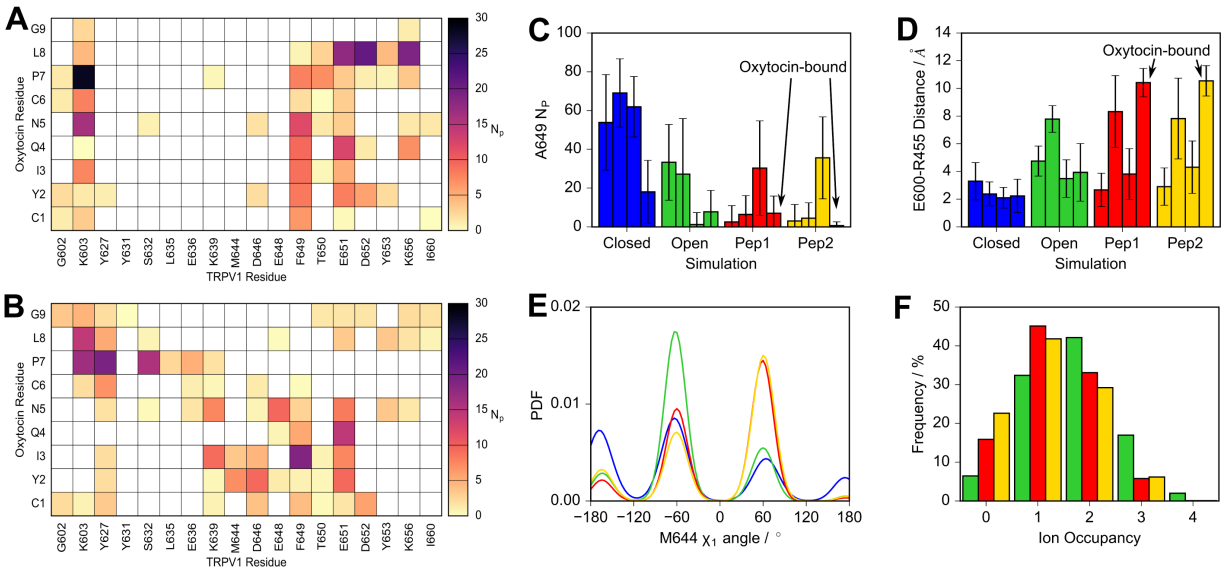

Figure S7: TRPV1-oxytocin interactions. **Related to Fig. 5.**

Contact maps displaying the number of interacting atom pairs (N_P) between TRPV1 and oxytocin in simulation Pep1 (**A**) and Pep2 (**B**), averaged over the simulation length, using a 4Å cut-off. **C**, Number of atomic interaction pairs between A649 and the other residues in the hydrophobic cluster. **D**, Minimum distance between E600 and E648 residues. In both, individual bars represent individual subunits in the TRPV1 channel, with those directly bound to oxytocin are shown. **E**, Probability density function of the M644 X_1 angle. **F**, Frequency distribution of the loading states of the SF2 site. Closed, Open, Pep1, and Pep2 simulations are shown in blue, green, red and yellow respectively.

Description	Coverage	# Peptides	# Unique Peptides
Transient receptor potential cation channel subfamily V member 1 OS=Rattus norvegicus GN=Trpv1	56.6307342	33	33
Keratin, type I cytoskeletal 10 OS=Homo sapiens GN=KRT10	45.2054795	25	21
Keratin, type II cytoskeletal 2 epidermal OS=Homo sapiens GN=KRT2	33.8028169	20	17
Keratin, type I cytoskeletal 9 OS=Homo sapiens GN=KRT9	33.2263242	9	9
Polyubiquitin-B (Fragment) OS=Homo sapiens GN=UBB	32.0388349	2	2
Protein S100-A7 OS=Homo sapiens GN=S100A7	30.6930693	3	3
Polyubiquitin-C (Fragment) OS=Homo sapiens GN=UBC	30.5970149	2	2
Lamin-B1 OS=Homo sapiens GN=LMNB1	29.5221843	14	14
Keratin, type II cytoskeletal 1 OS=Homo sapiens GN=KRT1	27.0186335	19	17
Trypsin OS=Sus scrofa	25.1082251	3	3
Histone H3.2 OS=Homo sapiens GN=HIST2H3A	23.5294117	1	1
Serine/threonine-protein kinase Nek3 (Fragment) OS=Homo sapiens GN=NEK3	18.2320442	1	1
Endoplasmin OS=Homo sapiens GN=HSP90B1	16.3138231	9	8
MICOS complex subunit MIC60 OS=Homo sapiens GN=IMMT	15.3305203	8	8
Keratin, type II cytoskeletal 6A OS=Homo sapiens GN=KRT6A	13.8297872	8	2
Heat shock protein HSP 90-beta OS=Homo sapiens GN=HSP90AB1	11.6022099	6	5
Ig gamma-2 chain C region OS=Homo sapiens GN=IGHG2	11.0429449	2	2
Keratin, type II cytoskeletal 5 OS=Homo sapiens GN=KRT5	11.0169495	7	1
Calnexin OS=Homo sapiens GN=CANX	9.96621626	4	4
60S ribosomal protein L3 OS=Homo sapiens GN=RPL3	8.43672456	2	2
Glial fibrillary acidic protein (Fragment) OS=Homo sapiens GN=GFAP	7.25806456	2	0
Hornerin OS=Homo sapiens GN=HRNR	7.22807015	3	3
Lysosome-associated membrane glycoprotein 2 OS=Homo sapiens GN=LAMP2	7.07317072	3	3
Keratin, type I cytoskeletal 16 OS=Homo sapiens GN=KRT16	5.72033893	3	2
Transitional endoplasmic reticulum ATPase OS=Homo sapiens GN=VCP	5.21091814	3	3
Cullin-1 OS=Homo sapiens GN=CUL1	4.89690726	1	1
Exocyst complex component 4 OS=Homo sapiens GN=EXOC4	3.90143732	1	1
Keratin, type II cytoskeletal 4 OS=Homo sapiens GN=KRT4	3.74531832	2	0
Keratin, type II cytoskeletal 80 OS=Homo sapiens GN=KRT80	2.43362839	1	1
Ceruloplasmin OS=Homo sapiens GN=CP	1.97183096	1	1
Leucine-rich PPR motif-containing protein, mitochondrial OS=Homo sapiens GN=LRPPRC	1.64992824	1	1

Table S1: The proteins identified using LC-MS/MS. Related to Figure 4.

The list of the proteins obtained from LC-MS/MS shows TRPV1 as the major protein purified from HEK-293 cells stably expressing the channel. The second group of abundant proteins includes keratins, as a typical contaminant factor during mass spectrometry. The peptide analysis was performed with the UniprotKB database, significance threshold $p < 0.05$, error range ±10 ppm. The TRPV1 protein was purified by immunoprecipitation with Myc antibodies.

Supplemental Information

Experimental Procedures

Computational studies: Influence on the TRPV1 activation state

Rearrangements in the outer pore region, encompassing the selectivity filter and adjacent extracellular loops, are a crucial attribute of TRPV1 activation, as evidenced by superposition of the apo and RTX/DkTx-bound structures. Three regions with marked differences are observed which show significant overlap with the oxytocin-binding site (Cao et al., 2013b): (1) A hydrophobic cluster constituted of residues V595, I599, T633, L637, F640, F649, T650, Y653, F659 and L663. The region is more compact in the *apo* state, relative to the RTX/DkTx-bound structure. (2) A charged cluster encompassing R455, K535, E600, and D654 residues. In the *apo* state, these residues are closely associated, whereas in the RTX/DkTx-bound structure, E600 is completely disengaged. (3) The selectivity filter (G643, M644, G645, D646). In the RTX/DkTx-bound structure, the selectivity filter is dilated and optimized for ion binding.

Accordingly, these regions were monitored throughout the simulation trajectories to assess the influence of oxytocin binding on the activation state of the receptor. F649 serves a dual-purpose as a key component of the hydrophobic cluster and oxytocin-binding interface. In the *apo* simulation, representative of the closed state, F649 forms frequent contacts with the hydrophobic residues, with an average of ~50 atomic pairs, and up to 140 formed at any time (Figure S7A). In the simulations initiated from the open state, F649 is predominantly detached from the cluster, but can spontaneously enter interacting conformations (Np > 20). When oxytocin is absent, two subunits have occupied the suggested closed state of the cluster; this is reduced to a single subunit when oxytocin is bound. Concurrently, the F649 residue in direct contact with oxytocin forms the lowest number of atomic contacts throughout, stabilizing the outer loop preceding S6 in a state representative of the open structure.

It is also apparent that oxytocin binding stabilizes surrounding loops in an open state, by interfering with cluster of charged residues R455, K535, E600, and D654. In the *apo* simulation, these residues are connected by salt-bridge interactions, with 2-4 Å between E600 and R455 (Figure S7B). In contrast, in the RTX/DkTx-bound structure, the charged entities of such residues are separated by approximately 10 Å. This distance is only maintained when E600 directly interacts with oxytocin, with frequent H-bonding observed with the Y2 residue of oxytocin in the Pep2 simulation. In the absence of an external binding partner, E600 is highly flexible and can spontaneously penetrate the charged cluster, forming the closed state.

Activation of TRPV1 is also accompanied by dilation of the selectivity filter, in order to cultivate ion permeation. The outward conduction mechanism can be described in terms of three binding sites; SC, the central cavity defined as the region in between residues I679 and Y671; SF1, localized on the carbonyl oxygen atoms of G643; and SF2, a region of high-field strength formed by negatively charged residues D646 and E648, and the carbonyl oxygen atoms of M644 and G645. Expansion of SF1 and SF2 are required to stimulate conduction, specifically via the distension of G643 carbonyl oxygen atoms and the downward movement of M644. The position of D646 is also optimized to facilitate ion coordination in the SF2 site.

The dynamics of the selectivity filter are seemingly perturbed in the SF2 locale as a result of oxytocin binding. Two rotameric states of M644 are observed in the *apo* and *holo* structures, displaying X_1 angles of -109 (up-state) and 39° (down-state) respectively. The up-state is prevalent in the presence of oxytocin (Figure S7C), whereas the unbound state predominantly occupies the down-state, suggesting oxytocin binding directly stabilizes this aspect of the open state selectivity filter. Although negligible differences are observed in the rotameric state of D646 residues, the occupancy of the SF2 site is markedly reduced when oxytocin is bound. The proportion of empty or singly occupied states is increased by 10-15 % in both oxytocin-bound simulations relative to the peptide-free simulation (Figure S7D), where doubly occupied states are most frequently observed.

The elevated occupancy of SF2 in the peptide-free simulation can be attributed to increased coordination of Na^+ ions to SF2 residues; in 45.7% of frames in the peptide-free simulations, bound ions interact with two or more SF2 residues, compared to 23.4% and 24.7% in the Pep1 and Pep2 simulations respectively. These coordination networks involve either D646 side-chains from adjacent subunits or D646 side-chains and M644/G645 backbone carbonyl atoms from the same subunit. It is possible that stabilization of the selectivity filter by oxytocin binding, as described previously, discourages the formation

of such networks and reduces the Na^+ binding affinity in this site. These observations suggest a direct link between oxytocin binding and permeation in the TRPV1 selectivity filter.

Mouse experiments

Adult male and female wild type, $TRPV1^{-/-}$, $TRPA1^{-/-}$, and $TRPM8^{-/-}$ mice were purchased from Jackson Laboratory, Maine, USA, and kept in the animal house located in the University of Illinois College of Medicine, as per protocols approved by the IACUC. The experiments were done under the protocol #627972. All the experiments were conducted using both genders at the age of 4-6 weeks old, to characterize their respective responsiveness to oxytocin. Mice were housed in a climate-controlled environment (22.8 ± 2.0 °C, 45–50% humidity) with a 12/12-light/dark cycle with access to designated diet and water *ad libitum*. All experiments were conducted at 22.8 ± 2.0 °C.

DRG neurons were isolated following the protocols (Malin et al., 2007; Sleigh et al., 2016), and maintained as we previously described (Cao et al., 2013a). Briefly, DRG neurons were cultured in the Primary Neuron Basal Medium, PNBM (Lonza Inc., Allendale, NJ). The fully supplemented medium contained 2 mM L-glutamine, 50 μg/ml gentamicin, 37 μg/ml amphotericin, and 2% NSF-1. For inhibition of Schwann cells and Glial cells, mitotic inhibitors were added to the medium (uridine 17.5 μg/ml and 5-fluoro-2-deoxyuridine 7.5 μg/ml). All the transfection experiments were done using Nucleofector(R) (Lonza), following the instructions from the manufacturer.

Cell culture

HEK-293 cells were maintained in minimal essential medium (MEM) solution (Invitrogen, San Diego, CA) supplemented with 10% fetal bovine serum (Invitrogen) and 1% penicillin/streptomycin. F-11 cells were cultured in DMEM/F12 medium +20% FBS, 0.2 mM L-glutamine, 100 μM sodium hypoxanthine, 400 nM aminopterin, 16 μM thymidine (HAT supplement), and penicillin/streptomycin at 37 °C, as previously described (Zakharian et al., 2009). The cells were transfected with the rat TRPV1 cDNA using the effectene reagent (Qiagen, Chatsworth, CA). The TRPV1 stable cell line was developed with TRPV1 tagged with *myc* on the N-terminus as previously described (Zakharian et al., 2009).

Intracellular Ca^{2+} measurements

The extracellular solution used in ratiometric $[Ca^{2+}]_i$ measurements contained (in mM) 137 NaCl, 5 KCl, 2 $CaCl_2$, 1 $MgCl_2$, 10 glucose and 10 HEPES, pH 7.4. Cells were incubated with 2 μM Fura-2 acetoxymethyl ester (Thermo Fisher Scientific, Waltham, MA) for 60 min at room temperature. The fluorescence signals of the cells grown on the coverslips were measured using alternating excitation at 340 and 380 nm and emission was detected at 510 nm. The ratio of fluorescence (340/380) was plotted against time. The obtained values of ratios from each coverslip were first analyzed and then the mean values of stimuli-induced signals were combined and statistically averaged values with mean errors were plotted in the summary graphs, the total number of measurements/cover slips (n) are indicated in the figure legend. The measurements were performed using a Photon Technology International (PTI) (Birmingham, NJ) imaging system mounted on Zeiss-AXIO Observed D1 microscope, equipped with a DeltaRAM excitation light source, or with a Ratiomaster 5 Imaging System (PTI) equipped with a Cool-snap HQ2 (Roper) Camera.

Whole-cell patch clamp recordings

The whole-cell patch clamp experiments were performed as previously described (Yudin et al., 2011; Zakharian et al., 2009). HEK-293T cells were cotransfected with rTRPV1 and eGFP with Lipofectamine 2000 according to manufacturer's protocol. Whole-cell patch clamp recordings were performed 48-72h post transfection at room temperature. The standard extracellular solution used in experiments contained (in mM) 135 NaCl, 5 KCl, 1 $MgCl_2$, 2 $CaCl_2$, 10 HEPES and 10 glucose, pH 7.4 (adjusted with NaOH). The pipette (intracellular) solution contained (in mM) 105 CsF, 35 NaCl, 8 KCl, 10 HEPES, 10 EGTA, pH 7.8 (adjusted with CsOH). Cell capacitance mean was 5.79±1pF, and access resistance <16MΩ. Data were acquired with an Axo-patch 200B amplifier (Molecular Devices), filtered with an 8-pole low-pass Bessel filter at 5 kHz and digitized at 10 kHz with a Digidata1320A interface and pClamp8.2 software (Molecular Devices). Pipettes were pulled from borosilicate glass and heat-polished to final resistances of 2-3.5MΩ. Currents are presented in terms of densities.

Preparation of the TRPV1 protein from HEK cells

HEK-293 cells stably expressing TRPV1 were grown to 70-80% confluence, washed, and collected with cold PBS. Cells were harvested and resuspended in NCB buffer, containing 500 mM NaCl, 50 mM NaH_2PO_4, 20 mM HEPES, 10% glycerol, pH 7.5, with addition of 1 mM of protease-inhibitor PMSF, 5 mM β-mercaptoethanol. Then the cells were lysed by freeze-thawing method and centrifuged at low speed to remove cell-debris and DNA. The supernatant was further centrifuged at 40,000 g for 2.5 h., and the pellet was resuspended in NCB buffer with addition of a protease inhibitor cocktail (Roche, Indianapolis, IN), 0.1% Nonidet P40 (Roche) and 0.5% dodecyl-maltoside (DDM) (CalBiochem). The suspension was incubated overnight at 4 °C on a shaker with gentle agitation and then centrifuged for 1 h. at 21,380 g. Further, the TRPV1 protein was purified by immuno-precipitation with anti-Myc-IgG conjugated to A/G protein magnetic beads (Pierce, Thermo Scientific), following the procedure provided by the manufacturer. All steps of purification were performed at 4 °C. For the planar lipid bilayers experiments the protein was eluted with Myc-peptide (150 μg/ml).

Mass spectrometry analysis

After the immunoprecipitation, TRPV1 prep was separated by SDS-PAGE and stained with coomassie blue. The bands was excised from the gel and digested with trypsin for mass spectrometry analysis according to Mann et al protocol (Shevchenko et al., 2006), with some modifications. Briefly, the gel bands were reduced with 0.5 M dithiothreitol and alkylated with 0.7 M iodoacetamide. Gel bands were digested with trypsin (Promega, Madison, WI) for 12 h at 37°C. Peptides were extracted from the gel bands with 100 μL of a 50% acetonitrile 5% formic acid solution. The extract was dried by vacuum centrifugation (SPD SpeedVac Thermo Electron Corp. Waltham, MA); the tryptic peptides were resuspended in 20 μL of a 3% acetonitrile, 0.5% formic acid solution.

Liquid chromatography-tandem mass mass spectrometry (LC-MS/MS) was performed using a nano flow liquid chromatography system (Ultimate3000, ThermoScientific) interfaced to a hybrid ion trap-orbitrap high-resolution tandem mass spectrometer (VelosPro, ThermoScientific) operated in data dependent acquisition (DDA) mode. Briefly, one micro-liter of each sample was injected onto a capillary column (4 μm Jupiter C18 manually packed on a 30 cm x 75um ID PicoFrit Column, New Objective) at a flow rate of 300 nl/min. Samples electro-sprayed at 1.2 kV using a dynamic nanospray ionization source. Chromatographic separation was carried out using 90 minute linear gradients (Mobile Phase A: 0.1% formic acid in MS-grade water, mobile phase B: 0.1% formic acid in MS-grade acetonitrile) from 3% B to 35% B over 60 minutes, then increasing to 95% B over 5 minutes. MS/MS spectra were acquired using both collision-induced dissociation (CID) and higher-energy collisional dissociation (HCD) for the top 15 peaks in the survey 30000-resolution MS scan. The .raw files were acquired (Xcalibur, ThermoFisher) and exported to Proteome Discoverer 2.0 (ThermoFisher) software for peptide and protein identification using SequestHT search algorithm (Full trypsin digestion with 2 maximum missed cleavages, 10 ppm precursor mass tolerance and 0.8 Da fragment mass tolerance). Database searching was done using the UniprotKB human database.

Planar lipid bilayer measurements

Planar lipid bilayers measurements were performed as previously described (Zakharian, 2013; Zakharian et al., 2010; Zakharian et al., 2009). Planar lipid bilayers were formed from a solution of synthetic 1-palmitoyl-2-oleoyl-glycero-3-phosphocoline (POPC) and 1-palmitoyl-2-oleoyl-glycero-3-phosphoethanolamine (POPE, Avanti Polar Lipids, Birmingham, AL) in ratio 3:1 in n-decane (Aldrich). The solution was used to paint a bilayer in an aperture of ~150μm diameter in a Delrin cup (Warner Instruments, Hamden, CT) between symmetric aqueous bathing solutions of 150 mM KCl, 0.02 mM $MgCl_2$, 1 μM $CaCl_2$, 20 mM Hepes, pH 7.2, at 22 °C. All salts were ultrapure (>99%) (Aldrich). Bilayer capacitances were in the range of 50-75 pF. After the bilayers were formed, the TRPV1 protein from micellar solution (20 ng/ml) was added by painting. Unitary currents were recorded with an integrating patch clamp amplifier (Axopatch 200B, Axon Instruments). The *trans* solution (voltage command side) was connected to the CV 201A head stage input, and the *cis* solution was held at virtual ground *via* a pair of matched Ag-AgCl electrodes. Currents through the voltage-clamped bilayers (background conductance < 1 pS) were filtered at the amplifier output (low pass, -3 dB at 10 kHz, 8-pole Bessel response). Data were secondarily filtered at 100 Hz through an 8-pole Bessel filter (950 TAF, Frequency Devices) and digitized at 1 kHz using an analog-to-digital converter (Digidata 1322A, Axon Instruments), controlled by pClamp10.3 software (Axon Instruments). Single-channel conductance events, all points' histograms, open

probability, and other parameters were identified and analyzed using the Clampfit10.3 software (Axon Instruments).

Defining the atomic interaction network between oxytocin and the TRPV1 ion channel

System Setup: The structures of the TRPV1 channel determined by single-particle cryo-electron microscopy in open (PDB: 3J5Q, resolution 3.8 Å) and closed (PDB: 3J5P, resolution 3.28 Å) states were used as atomic models of the system. To predict the sequence of the β-strand in the C-terminal domain (denoted 752-762 in the PDB model), all possible models of residues 720-751 were built and validated using FASTCONTACT, advocating that residues 741-751 are the likely occupants of the β-strand (Camacho and Zhang, 2005). This assignment was further supported by alignment with the TRPV2 channel, where the resolved structure demonstrates conserved residues in the analogous position (Zubcevic et al., 2016). The remaining missing loop in the C-terminal domain (residues 720 to 740), as well as the unresolved segment of the S2-S3 loop (503 to 507), were modelled using Modloop (Fiser and Sali, 2003). Thus, the final channel model contained residues 111 to 751, with the N- and C- termini acetylated and methylated respectively and default protonation states used for ionisable residues (Li et al., 2005). The double-knot toxin (DkTx) and the vanilloid resiniferatoxin (RTx) were removed from the open state. Structural alignment of DkTx and oxytocin was performed to predicate the binding site of oxytocin in the outer pore region, resulting in the placement of four oxytocin molecules in both open and closed systems. SOLVATE1.0 was used to fill the internal cavities of the proteins, which were inserted into a pre-equilibrated lipid bilayer of 1-palmitoyl-2-oleoyl-sn-glycero-3-phosphocholine (POPC) molecules, generated using the Membrane Plugin of VMD (Humphrey et al., 1996). The systems were then solvated to produce a cubic water box, and NaCl was added, using the Autoionise Plugin of VMD (Humphrey et al., 1996), to neutralize and mimic the biological ionic concentration of 150 mM. The resulting system size was approximately 300,000 atoms.

Initially, MD simulations of both the open and closed states of TRPV1 were performed for 200 ns. Prolonged oxytocin binding was observed in the open state, thus this simulation was extended for a further 100 ns. The predominant binding pose was replicated in each subunit in an independent simulation, 200 ns in length. A control simulation of TRPV1 in the open state, without oxytocin, was also performed for 200 ns, to assess the effect of bound oxytocin.

The FlexPepDock Server, a component of the Rosetta program, was used to predict further oxytocin-binding poses in the open and closed states (London et al., 2011; Raveh et al., 2010).

Molecular Dynamics (MD) Simulations

NAMD2.9 was employed to perform MD simulations (Phillips et al., 2005). The CHARMM22 force field (with the CMAP correction) was used to describe the TRPV1 channel and the oxytocin peptide, CHARMM36 for lipids,(Klauda et al., 2010) TIP3P(Jorgensen et al., 1983) model for water, and standard ion parameters.(Beglov and Roux, 1994) The Particle Mesh Ewald method was used for the treatment of periodic electrostatic interactions, with an upper threshold of 1 Å for grid spacing (Darden et al., 1993). Electrostatic and van der Waals forces were calculated every timestep. A cut-off distance of 12 Å was used for van der Waals forces. A switching distance of 10 Å was chosen to smoothly truncate the non-bonded interactions. Only atoms in a Verlet pair list with a cut-off distance of 13.5 Å (reassigned every 20 steps) were considered (Verlet, 1967). The SETTLE algorithm was used to constrain all bonds involving hydrogen atoms to allow the use of a 2 fs time step throughout the simulation (Miyamoto and Kollman, 1992). The Nose-Hoover-Langevin piston method was employed to control the pressure with a 200 fs period, 50 fs damping constant and a desired value of 1 atmosphere (Feller et al., 1995; Martyna et al., 1994). The system was coupled to a Langevin thermostat to sustain a temperature of 310 K throughout.

Equilibration Protocol

The systems were subject to 10,000 steps of minimization with the protein backbone atoms restrained, and subsequently equilibrated for a total of 2.5 ns. Each equilibration step was undertaken for 500 ps, with restraints removed systematically: (i) lipid tails, (ii) water and lipid headgroups, (iii) oxytocin molecules, (iv) TRPV1 side-chain atoms, and (v) TRPV1 backbone atoms of residues 720 to 740 and 503 to 507.

Nocifensive behavior in mice

Animals: Adult male C57BL/6J mice were used. Animals were housed in group cages in a temperature-controlled environment on a 12-hour light/dark cycle and supplied with water and food *ad libitum*. The experiments were performed according to the guideline of the International Association or the Study of Pain and approved by the internal review board of the university and the local district government.

Chemicals: The following chemicals were used: capsaicin (Sigma-Aldrich) and oxytocin (Cayman Chemical). Capsaicin was dissolved in ethanol for preparing concentrated stock solutions of 10 mM and working solution was diluted in saline prior to the use. Oxytocin was dissolved in *aqua destillata* to provide a stock solution of 1 mM kept at -20 ^{o}C in BSA pretreated Eppendorf cups and added to the capsaicin solution at its final concentration of 4 µg in 20 µL.

Behavior test: Animals were placed in an observation apparatus onto a transparent plexiglass surface with individual chambers of 9 x 9 x 15 cm. Mice were adapted to the equipment for one hour per day on 3 subsequent days previous to the behavioral test. Mice were anesthetized with 3% sevoflurane, and capsaicin (1.6 µg/paw in a volume of 20 µL) (Sakurada et al., 1992) or combination of capsaicin and oxytocin solution was injected intracutaneously into mice hind paw with a 100 µL Hamilton microsyringe and a 30 gauge needle. After the injection, animals (6 mice each time) were put in the observation apparatus, and their behavior was recorded from the bottom side with a high-resolution camera (C920 HD Pro Webcam, Logitech) for 30 minutes. Videos were analyzed offline with the experimenter blinded to the groups.

Statistical analysis

Statistical analysis was performed using Origin 9.0 software (Microcal Software Inc., Northampton, MA, USA). Statistical significance was calculated using one-way ANOVA followed by Fisher's LSD test, or Student's t-test and data were expressed as mean ± SEM. $P < 0.05$ was considered to be significant. In all figures, statistical significance is labeled the following way: *P <0.05, **P <0.01, ***P <0.001, and ****P <0.0001.

Supplementary References:

Beglov, D., and Roux, B. (1994). Finite representation of an infinite bulk system: Solvent boundary potential for computer simulations. The Journal of Chemical Physics *100*, 9050-9063.

Camacho, C.J., and Zhang, C. (2005). FastContact: rapid estimate of contact and binding free energies. Bioinformatics *21*, 2534-2536.

Cao, C., Yudin, Y., Bikard, Y., Chen, W., Liu, T., Li, H., Jendrossek, D., Cohen, A., Pavlov, E., Rohacs, T., *et al.* (2013a). Polyester modification of the mammalian TRPM8 channel protein: implications for structure and function. Cell reports *4*, 302-315.

Cao, E., Liao, M., Cheng, Y., and Julius, D. (2013b). TRPV1 structures in distinct conformations reveal activation mechanisms. Nature *504*, 113-118.

Darden, T., York, D., and Pedersen, L. (1993). Particle mesh Ewald: An N·log(N) method for Ewald sums in large systems. The Journal of Chemical Physics *98*, 10089-10092.

Feller, S.E., Zhang, Y., Pastor, R.W., and Brooks, B.R. (1995). Constant pressure molecular dynamics simulation: the Langevin piston method. The Journal of chemical physics *103*, 4613-4621.

Fiser, A., and Sali, A. (2003). ModLoop: automated modeling of loops in protein structures. Bioinformatics (Oxford, England) *19*, 2500-2501.

Humphrey, W., Dalke, A., and Schulten, K. (1996). VMD: Visual molecular dynamics. Journal of Molecular Graphics *14*, 33-38.

Jorgensen, W.L., Chandrasekhar, J., Madura, J.D., Impey, R.W., and Klein, M.L. (1983). Comparison of simple potential functions for simulating liquid water. The Journal of chemical physics *79*, 926-935.

Klauda, J.B., Venable, R.M., Freites, J.A., O'Connor, J.W., Tobias, D.J., Mondragon-Ramirez, C., Vorobyov, I., MacKerell Jr, A.D., and Pastor, R.W. (2010). Update of the CHARMM all-atom additive force field for lipids: validation on six lipid types. The journal of physical chemistry B *114*, 7830-7843.

Li, H., Robertson, A.D., and Jensen, J.H. (2005). Very fast empirical prediction and rationalization of protein pKa values. Proteins *61*, 704-721.

London, N., Raveh, B., Cohen, E., Fathi, G., and Schueler-Furman, O. (2011). Rosetta FlexPepDock web server--high resolution modeling of peptide-protein interactions. Nucleic acids research *39*, W249-253.
Lukacs, V., Rives, J.M., Sun, X., Zakharian, E., and Rohacs, T. (2013). Promiscuous activation of transient receptor potential vanilloid 1 (TRPV1) channels by negatively charged intracellular lipids: the key role of endogenous phosphoinositides in maintaining channel activity. J Biol Chem *288*, 35003-35013.
Malin, S.A., Davis, B.M., and Molliver, D.C. (2007). Production of dissociated sensory neuron cultures and considerations for their use in studying neuronal function and plasticity. Nat Protoc *2*, 152-160.
Martyna, G.J., Tobias, D.J., and Klein, M.L. (1994). Constant pressure molecular dynamics algorithms. The Journal of Chemical Physics *101*, 4177-4189.
Miyamoto, S., and Kollman, P.A. (1992). SETTLE: an analytical version of the SHAKE and RATTLE algorithm for rigid water models. J Comput Chem *13*, 952-962.
Phillips, J.C., Braun, R., Wang, W., Gumbart, J., Tajkhorshid, E., Villa, E., Chipot, C., Skeel, R.D., Kale, L., and Schulten, K. (2005). Scalable molecular dynamics with NAMD. Journal of computational chemistry *26*, 1781-1802.
Raveh, B., London, N., and Schueler-Furman, O. (2010). Sub-angstrom modeling of complexes between flexible peptides and globular proteins. Proteins *78*, 2029-2040.
Sakurada, T., Katsumata, K., Tan-No, K., Sakurada, S., and Kisara, K. (1992). The capsaicin test in mice for evaluating tachykinin antagonists in the spinal cord. Neuropharmacology *31*, 1279-1285.
Shevchenko, A., Tomas, H., Havlis, J., Olsen, J.V., and Mann, M. (2006). In-gel digestion for mass spectrometric characterization of proteins and proteomes. Nat Protoc *1*, 2856-2860.
Sleigh, J.N., Weir, G.A., and Schiavo, G. (2016). A simple, step-by-step dissection protocol for the rapid isolation of mouse dorsal root ganglia. BMC Res Notes *9*, 82.
Verlet, L. (1967). Computer" experiments" on classical fluids. I. Thermodynamical properties of Lennard-Jones molecules. Physical review *159*, 98.
Yudin, Y., Lukacs, V., Cao, C., and Rohacs, T. (2011). Decrease in phosphatidylinositol 4,5-bisphosphate levels mediates desensitization of the cold sensor TRPM8 channels. The Journal of physiology *589*, 6007-6027.
Zakharian, E. (2013). Recording of ion channel activity in planar lipid bilayer experiments. Methods in molecular biology *998*, 109-118.
Zakharian, E., Cao, C., and Rohacs, T. (2010). Gating of transient receptor potential melastatin 8 (TRPM8) channels activated by cold and chemical agonists in planar lipid bilayers. The Journal of neuroscience : the official journal of the Society for Neuroscience *30*, 12526-12534.
Zakharian, E., Thyagarajan, B., French, R.J., Pavlov, E., and Rohacs, T. (2009). Inorganic polyphosphate modulates TRPM8 channels. PLoS One *4*, e5404.
Zubcevic, L., Herzik Jr, M.A., Chung, B.C., Liu, Z., Lander, G.C., and Lee, S.-Y. (2016). Cryo-electron microscopy structure of the TRPV2 ion channel. Nat Struct Mol Biol *23*, 180-186.